International Journal of Heat and Mass Transfer 139 (2019) 1065–1076

Contents lists available at ScienceDirect

International Journal of Heat and Mass Transfer

journal homepage: www.elsevier.com/locate/ijhmt

A liquid plug moving in an annular pipe – Heat transfer analysis

Yadi Cao, Xuan Gao, Ri Li *

School of Engineering, University of British Columbia, Kelowna, British Columbia V1V 1V7, Canada

ARTICLE INFO

Article history:
Received 1 April 2019
Received in revised form 20 May 2019
Accepted 26 May 2019
Available online 1 June 2019

ABSTRACT

Different from a fully developed continuous flow in an annular pipe, a liquid plug moving in an annular pipe generates two toroidal vortexes, which cause radial transport that enhances heat transfer. The fully developed heat transfer of the concentric plug is studied for three types of thermal wall conditions: inner-flux, outer-flux, and isothermal. The fully developed heat transfer of the continuous flow is analytically solved for the same thermal wall conditions. The comparison of heat transfer is made between the plug and the continuous flow. Two heat transfer mechanisms, boundary layer transport and radial transport, are considered to explain the heat transfer enhancement. If the radial transport is weak, the plug shows similar heat transfer performance to the continuous flow, which is dominated by the boundary layer transport. The heat transfer enhancement relies on the radial transport, which increases with decreasing the inner radius, decreasing the plug length, and increasing the Peclet number.

1. Introduction

Compact heat exchangers and compact cold plates based on micro- or meso-channel liquid flows have been finding increased applications [1,2]. One major driver is the continuous increase of power density in microelectronic and power-electronic devices, for which effective cooling needs to be applied to small areas to handle high heat fluxes. The high cooling capability is attributed to the large surface-to-volume ratio of the small-scale channels. However, on the other hand, the large surface-to-volume ratio means small hydraulic diameter, which make it difficult to increase the flow Reynolds number due to the penalty of pressure drop increase. This poses difficulty to increasing the heat transfer coefficient for these small-scale channel flows.

To enhance the heat transfer, efforts have been put on modifying the channel in order to change the flow behavior. Some of the efforts include using curved channels or other channels with varied passages [3,4] and adding small fins on the channel wall [5,6]. Another method is to change the type of flow from continuous flow to plug flow. The continuous flow means the channel is entirely filled with one liquid fluid. In a plug flow, the liquid fluid is segmented by another immiscible fluid, which could be liquid or gas. Due to the significant capillary effect associated with the small channel size, each liquid segment occupies the entire cross-section of the channel and looks like a moving plug. When such a liquid plug is moving in a circular channel, the wall friction causes vortex inside the plug, which provides advection in radial direction [7–9]. The heat transfer enhancement using plug flow has attracted much attention recently [10].

A number of experimental studies on plug flows have been reported. Gas-liquid plug moving in a vertical circular tube with constant heat flux was studied [11,12], and the effects of the capillary number and the Graetz number were investigated. For the gas-liquid plug flow in a circular tube with constant heat flux, the pressure drop penalty caused by the plug flow was measured and compared to the Nusselt number increment, showing more significant enhancement of heat transfer than the pressure drop penalty [13]. Infrared camera was used to measure the continuous temperature distribution of the outer surface of a circular tube containing a constant gas-liquid plug flow [14,15]. Experimental study on liquid-liquid plug flow has been conducted to study the flow and thermal fields simultaneously using an IR camera and a high-speed camera [16]. It was found the Nusselt number is highly dependent on the plug length. The heat transfer coefficient of air–water plug flow in horizontal microchannel with different configurations of heated areas was studied using an array of heaters and resistance temperature detectors instrumented inside the channel [17].

Numerical approaches have been widely used for the study on plug flows, due to the measurement limitation of the experimental approaches for microchannels. For the numerical simulation of plug flows, choosing the appropriate frame of reference is important, because it significantly affects the required computational resource. It has been shown that the moving frame technique took only 1/150 of the computational time needed by the stationary domain technique [18,19], and the results from the two techniques showed good agreement. In order to deal with the interface shape

* Corresponding author.
E-mail address: sunny.li@ubc.ca (R. Li).

https://doi.org/10.1016/j.ijheatmasstransfer.2019.05.088
0017-9310/

Nomenclature

A_n, B_n, C_n, D_h coefficients
h heat transfer coefficient of continuous flow with isothermal condition
h_i heat transfer coefficient of continuous flow with inner-flux condition
h_o heat transfer coefficient of continuous flow with outer-flux condition
h_p heat transfer coefficient of plug with isothermal condition
$h_{p,i}$ heat transfer coefficient of plug with inner-flux condition
$h_{p,o}$ heat transfer coefficient of plug with outer-flux condition
I first-kind modified Bessel function
k thermal conductivity
K second-kind modified Bessel function
l plug length
q'' heat flux
Q' circulation rate per unit length of the plug
r r-axis in cylindrical coordinate system
r_i inner radius of plug
r_o outer radius of plug
r_c radial location of border between inner and outer vortexes
R radial location of pipe wall
T temperature
T_i constant inner wall temperature
T_o constant outer wall temperature
T_{ref} constant reference temperature
ΔT_{std} characteristic temperature difference
$\widehat{T}_a$ an arbitrary local temperature
$\widehat{T}_m$ mean temperature of continuous flow
$\widehat{T}_{p,m}$ mean temperature of the plug
u_z velocity in z-direction
u_r velocity in r-direction
U velocity of plug moving in pipe
z z-axis in cylindrical coordinate system

Symbols
$\hat{}$ dimensionless
$\bar{}$ average

Greek symbols
α thermal diffusivity
α_n eigenvalue
η radius ratio (or non-dimensional inner radius)
μ dynamic viscosity
ρ density

Non-dimensional group parameters
Nu Nusselt number for continuous flow with isothermal condition
Nu_i Nusselt number for continuous flow with inner-flux condition
Nu_{i,D_h} Nusselt number based on hydraulic diameter for inner-flux condition
Nu_{o,D_h} Nusselt number based on hydraulic diameter for outer-flux condition
Nu_o Nusselt number for continuous flow with outer-flux condition
Nu_p Nusselt number for plug with isothermal condition
$Nu_{p,i}$ Nusselt number for plug with inner-flux condition
$Nu_{p,o}$ Nusselt number for plug with outer-flux condition
Pe Peclet number
Re Reynolds number

of the plug, especially for channels that cannot be simplified into 2D, the Level Set method [20,21] and the Volume of Fluid method [22,23] are commonly used, although the two methods require much computational time. Recently, there has been much work using a combined approach, in which the flow field is analytically solved based on the Stokes assumption, and the flow results are put into the heat transfer computation based on the finite volume method [8,24,25]. This combined approach has been proved effective and efficient, and is adopted in the present work.

The heat transfer of internal flows usually consists of entrance region and fully developed region. A few studies on plug flows have shown that the entrance region is around 20 times as long as the hydraulic diameter of the channel [8,23,24]. For many microchannels, the length-to-diameter ratio is around the order of magnitude of 1000. Hence, it is useful to focus on the fully developed heat transfer of plug flows. However, obtaining the fully developed heat transfer from transient computation takes much computational time. In the present work, the transient term in the heat transfer governing equation is replaced with a constant term so that the fully developed heat transfer performance can be computed based on a non-transient equation.

Annular channels are commonly seen in many applications, and one major application is the concentric tube (tube-in-tube) heat exchanger. Recently, there has been attention to the convection heat transfer in small concentric tubes [26-31]. One way to enhance the convection in small concentric tubes is to use plug flow instead of continuous flow. There has been no study on the heat transfer of plug flow in an annular pipe. The present work is focused on the fully developed heat transfer of a liquid plug in an annular pipe. The analytically solved flow field is put into the numerical computation of heat transfer, and the computation is done by using the finite volume method to compute the non-transient governing equation.

The fluid mechanics of a liquid plug moving in an annular pipe has been solved [32]. The present work focuses on the heat transfer aspect of the liquid plug. Fig. 1 schematically shows a liquid plug with a length l is moving at a constant velocity U in an annular pipe, which has an inner radius r_i and an outer radius r_o. The cylindrical coordinates system is attached to the plug as shown in Fig. 1. The plug is assumed to have flat ends so that surface tension is not considered. Hence, the fluid properties relevant to the flow dynamics include the density ρ and the dynamic viscosity μ.

The plug can be described by three dimensionless parameters, which are

$$\eta = \frac{r_i}{r_o}; \quad \hat{l} = \frac{l}{r_o}; \quad Re = \frac{\rho U r_o}{\mu} \tag{1}$$

Here η is the radius ratio, and is also called the dimensionless inner radius. For $\eta \to 0$, the annular pipe approaches a circular pipe, while for $\eta \to 0$ the annular pipe approaches two parallel plates. The dimensionless length is denoted by $\hat{l}$, and Re is the Reynolds number. Additionally, the coordinates and velocities are normalized as

$$\hat{z} \equiv \frac{z}{r_o}; \quad \hat{r} \equiv \frac{r}{r_o}; \quad \hat{u}_z \equiv \frac{u_z}{U}; \quad \hat{u}_r \equiv \frac{u_r}{U} \tag{2}$$

If $Re(1-\eta) \ll 1$, the plug flow was solved as a Stokes flow [32]. The obtained velocity solutions were independent of the Reynolds number, which appeared only in the pressure solution. As shown in

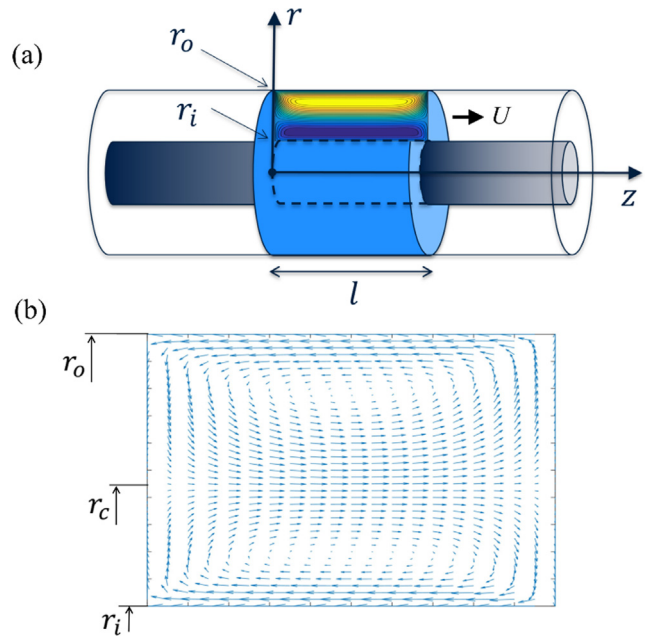

Fig. 1. (a) Schematic of a liquid plug moving in an annular pipe. In the floor-attached frame reference that is not shown, the plug velocity is U. (b) Velocity vectors show two vortexes in the plug.

Fig. 1b, the interaction with the two concentric walls of the annular pipe results in two toroidal vortexes within the concentric plug (see Fig. 1b). It was found that the two vortexes border at

$$r_c = (r_i r_o)^{0.5} \tag{3}$$

The circulation caused by the two vortexes generates flow in radial direction. The circulation volume rate per unit plug length was found to satisfy

$$Q' = \frac{0.1973\left(r_o^2 - r_i^2\right)U}{l} \tag{4}$$

The velocity solutions in the dimensionless form are [32]

$$\hat{u}_z(\hat{z},\hat{r}) = \sum_{n=1,3,5\ldots}^{\infty} \alpha_n[A_n\hat{r}\mathrm{I}_1(\alpha_n\hat{r}) + B_n\mathrm{I}_0(\alpha_n\hat{r}) - C_n\hat{r}\mathrm{K}_1(\alpha_n\hat{r}) - D_n\mathrm{K}_0(\alpha_n\hat{r})]\sin(\alpha_n\hat{z}) \tag{5}$$

$$\hat{u}_r(\hat{z},\hat{r}) = \sum_{n=1,3,5\ldots}^{\infty} -\alpha_n[A_n\hat{r}\mathrm{I}_2(\alpha_n\hat{r}) + B_n\mathrm{I}_1(\alpha_n\hat{r}) + C_n\hat{r}\mathrm{K}_2(\alpha_n\hat{r}) + D_n\mathrm{K}_1(\alpha_n\hat{r})]\cos(\alpha_n\hat{z}) \tag{6}$$

Here $\mathbf{I}_0$, $\mathbf{I}_1$ and $\mathbf{I}_2$ are the 0th, 1st, and 2nd order of the first-kind modified Bessel functions, respectively. Also, $\mathbf{K}_0$, $\mathbf{K}_1$ and $\mathbf{K}_2$ are the 0th, 1st, and 2nd order of the second-kind modified Bessel functions, respectively. The coefficients, A_n, B_n, C_n, and D_n, should be determined from

$$\begin{pmatrix} \eta\mathrm{I}_2(\alpha_n\eta) & \mathrm{I}_1(\alpha_n\eta) & \eta\mathrm{K}_2(\alpha_n\eta) & \mathrm{K}_1(\alpha_n\eta) \\ \mathrm{I}_2(\alpha_n) & \mathrm{I}_1(\alpha_n) & \mathrm{K}_2(\alpha_n) & \mathrm{K}_1(\alpha_n) \\ \eta\mathrm{I}_1(\alpha_n\eta) & \mathrm{I}_0(\alpha_n\eta) & -\eta\mathrm{K}_1(\alpha_n\eta) & -\mathrm{K}_0(\alpha_n\eta) \\ \mathrm{I}_1(\alpha_n) & \mathrm{I}_0(\alpha_n) & -\mathrm{K}_1(\alpha_n) & -\mathrm{K}_0(\alpha_n) \end{pmatrix} \begin{pmatrix} A_n \\ B_n \\ C_n \\ D_n \end{pmatrix} = \begin{pmatrix} 0 \\ 0 \\ -\frac{2\eta}{l\alpha_n}\left[1-(-1)^n\right] \\ -\frac{2\eta}{l\alpha_n}\left[1-(-1)^n\right] \end{pmatrix} \tag{7}$$

where $\alpha_n = n\pi/\hat{l}$ is the eigenvalue.

In the present work, Eqs. (5)–(7) will be used to solve the *fully developed heat transfer* of a liquid plug moving in an annular pipe with different thermal wall conditions. To analyze the heat transfer enhancement, the heat transfer of the plug flow will be compared to the fully developed heat transfer of the continuous flow in an annular pipe. The heat transfer of the continuous flow is solved in the Appendix A.

2. General consideration

To analyze the heat transfer of a liquid plug, the thermal properties of the plug fluid need to be included. Here we choose the thermal conductivity, k, and the thermal diffusivity α. To fully describe the plug, in addition to the three dimensionless parameters defined in Eq. (1), another parameter, the Peclet number, is defined as

$$Pe = \frac{Ur_o}{\alpha} \tag{8}$$

The thermal conductivity will appear in the dimensional heat transfer.

In the present work, three types of thermal wall conditions are considered, as shown in Fig. 2. Fig. 2a shows a uniform heat flux, $-q''$, is maintained at the outer surface, while the inner surface is maintained adiabatic. This is referred to the *outer-flux* condition, which is

$$k\left.\frac{\partial T}{\partial r}\right|_{r=r_o} = q''; \quad \left.\frac{\partial T}{\partial r}\right|_{r=r_i} = 0 \tag{9}$$

Fig. 2b shows a uniform heat flux, q'', is maintained at the inner surface, while the outer surface is adiabatic. This is referred to the *inner-flux* condition, which is

$$\left.\frac{\partial T}{\partial r}\right|_{r=r_o} = 0; \quad -k\left.\frac{\partial T}{\partial r}\right|_{r=r_i} = q'' \tag{10}$$

Fig. 2c shows that two different constant temperatures, T_i and T_o, are maintained at the inner and outer surfaces of the plug. This is referred to as the *isothermal* condition, which is

$$T(r = r_i, z, t) = T_i; \quad T(r = r_o, z, t) = T_o \tag{11}$$

The governing equation of heat transfer in the cylindrical coordinates system is

$$\frac{\partial T}{\partial t} + \frac{u_r}{r}\frac{\partial (Tr)}{\partial r} + u_z\frac{\partial T}{\partial z} = \alpha\left[\frac{1}{r}\frac{\partial}{\partial r}\left(r\frac{\partial T}{\partial r}\right) + \frac{\partial^2 T}{\partial z^2}\right] \tag{12}$$

In reality, the front and rear ends of the plug are in contact with gas plugs. Due to negligible heat transfer with the gas, the two ends of the plug are assumed to be adiabatic, which is

$$\left.\frac{\partial T}{\partial z}\right|_{z=0} = 0; \quad \left.\frac{\partial T}{\partial z}\right|_{z=l} = 0 \tag{13}$$

In addition to Eq. (2), we define dimensionless time and temperature as

$$\hat{t} \equiv \frac{tU}{r_o}; \quad \hat{T} \equiv \frac{T - T_{ref}}{\Delta T_{std}} \tag{14}$$

Here T_{ref} is a constant reference temperature, and ΔT_{std} is a characteristic temperature difference. Both T_{ref} and ΔT_{std} will be specifically defined for each type of thermal wall conditions. Applying Eqs. (2) and (14) to Eq. (12) gives

$$\frac{\partial \hat{T}}{\partial \hat{t}} + \frac{\hat{u}_r}{\hat{r}}\frac{\partial\left(\hat{T}\hat{r}\right)}{\partial \hat{r}} + \hat{u}_z\frac{\partial \hat{T}}{\partial \hat{z}} = \frac{1}{Pe}\left[\frac{1}{\hat{r}}\frac{\partial}{\partial \hat{r}}\left(\hat{r}\frac{\partial \hat{T}}{\partial \hat{r}}\right) + \frac{\partial^2 \hat{T}}{\partial \hat{z}^2}\right] \tag{15}$$

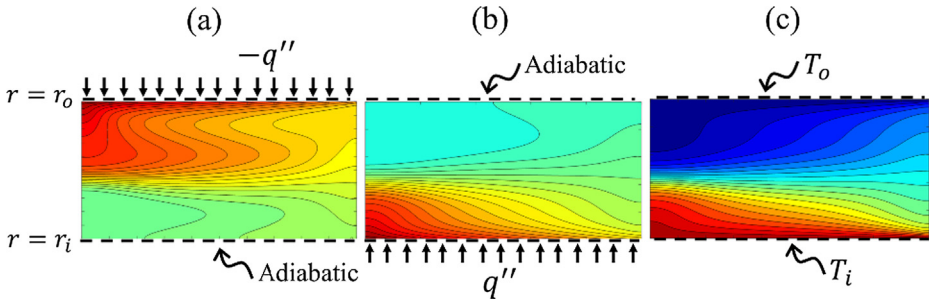

Fig. 2. Three types of thermal wall conditions are studied: (a) Outer-flux condition; (b) Inner-flux condition; (c) Isothermal condition.

The solutions for $\hat{u}_r$ and $\hat{u}_z$ are given by Eqs. (5)–(7). The boundary condition at the two ends of the plug can be rewritten as

$$\left.\frac{\partial \hat{T}}{\partial \hat{z}}\right|_{\hat{z}=0} = 0; \quad \left.\frac{\partial \hat{T}}{\partial \hat{z}}\right|_{\hat{z}=\hat{l}} = 0 \tag{16}$$

The focus of the present work is on the fully developed heat transfer of the plug under the three types of thermal wall conditions. The fully developed heat transfer means that the moving plug has fully developed both hydro-dynamically and thermally. The fully developed heat transfer will be defined and discussed. It will be shown that the transient term in Eq. (15) can be replaced with a non-transient term, which varies with the wall boundary condition. As a result, Eq. (15) will become a steady state equation, which, with Eqs. (5)–(7) inserted, is solved using the finite volume method implemented in MATLAB2016A. The meshing resolution is $(1-\eta)/200$ for $\hat{r}$ and $\hat{l}/400$ for $\hat{z}$, which was determined based on mesh independency tests. One test will be shown in Section 3.1.

To determine the non-transient term for replacing the transient term in Eq. (15), we need to first define the fully developed heat transfer. Integrating Eq. (15) over the entire volume of the plug and applying the divergence theorem gives

$$\frac{\partial}{\partial \hat{t}}\int_\eta^1\int_0^{\hat{l}} \hat{T} 2\pi \hat{r} d\hat{r} d\hat{z} = \frac{1}{Pe}\int_0^{\hat{l}}\left(2\pi \left.\frac{\partial \hat{T}}{\partial \hat{r}}\right|_{\hat{r}=1} - 2\pi\eta \left.\frac{\partial \hat{T}}{\partial \hat{r}}\right|_{\hat{r}=\eta}\right) d\hat{z} \tag{17}$$

where Eq. (16) has been used. Considering the volume integration on the left hand side, we introduce a volume average temperature of the plug given by

$$\hat{T}_{p,m} = \frac{1}{\pi(1-\eta^2)\hat{l}}\int_\eta^1\int_0^{\hat{l}} \hat{T} 2\pi \hat{r} d\hat{r} d\hat{z} \tag{18}$$

Hence, Eq. (17) can be rewritten as

$$\frac{d\hat{T}_{p,m}}{d\hat{t}} = \frac{1}{(1-\eta^2)\hat{l}}\frac{2}{Pe}\int_0^{\hat{l}}\left[\left.\frac{\partial \hat{T}}{\partial \hat{r}}\right|_{\hat{r}=1} - \eta\left.\frac{\partial \hat{T}}{\partial \hat{r}}\right|_{\hat{r}=\eta}\right] d\hat{z} \tag{19}$$

When heat transfer has fully developed, the relative shape of the temperature profile will no longer change (see the temperature contours shown in Fig. 2). This axiom has been used to derive the fully developed heat transfer of continuous flows [33].The relative temperature contour can be expressed by

$$\frac{\hat{T}_a(\hat{r}_a,\hat{z}_a,\hat{t}) - \hat{T}(\hat{r},\hat{z},\hat{t})}{\hat{T}_a(\hat{r}_a,\hat{z}_a,\hat{t}) - \hat{T}_{p,m}(\hat{t})} = f(\hat{r},\hat{z},\hat{r}_a,\hat{z}_a) \tag{20}$$

Here $\hat{T}_a$ is a local temperature at an arbitrary location $(\hat{r}_a,\hat{z}_a)$. Since the relative temperature contour is constant, we take time derivative of Eq. (20) and get

$$\frac{\partial \hat{T}}{\partial \hat{t}} = \frac{d\hat{T}_a}{d\hat{t}} + \frac{\hat{T}_a - \hat{T}}{\hat{T}_a - \hat{T}_{p,m}}\left(\frac{d\hat{T}_{p,m}}{dt} - \frac{d\hat{T}_a}{d\hat{t}}\right) \tag{21}$$

Next we will apply Eq. (21) to each type of wall condition to determine the non-transient term that can be used to replace the transient term in Eq. (15). We will then numerically compute Eq. (15), and compare the fully developed heat transfer of the plug with that of the continuous flow. The fully developed heat transfer of the continuous flow is solved in the Appendix A.

3. Iso-flux wall conditions

When either the inner surface or the outer surface is at an iso-flux condition and the other surface is adiabatic, we define a characteristic temperature difference $\Delta T_{std} = q'' r_o/k$. Hence, the dimensionless temperature given in Eq. (14) can be rewritten as

$$\hat{T} \equiv \frac{T - T_{ref}}{q'' r_o/k} \tag{22}$$

There is no need to specify the reference temperature T_{ref} as the heat transfer below will be based on temperature difference. The *outer-flux* condition given by Eq. (9) becomes

$$\left.\frac{\partial \hat{T}}{\partial \hat{r}}\right|_{\hat{r}=1} = 1; \quad \left.\frac{\partial \hat{T}}{\partial \hat{r}}\right|_{\hat{r}=\eta} = 0 \tag{23}$$

The *inner-flux* condition given by Eq. (10) becomes

$$\left.\frac{\partial \hat{T}}{\partial \hat{r}}\right|_{\hat{r}=1} = 0; \quad \left.\frac{\partial \hat{T}}{\partial \hat{r}}\right|_{\hat{r}=\eta} = -1 \tag{24}$$

3.1. Outer-flux condition

A uniform heat flux is maintained at the outer surface of the plug, while the inner surface is insulated. The heat transfer at the wall-fluid interface is

$$-\left.\frac{\partial \hat{T}}{\partial \hat{r}}\right|_{\hat{r}=1} = Nu_{p,o}\left[\hat{T}(1,\hat{z},\hat{t}) - \hat{T}_{p,m}(\hat{t})\right] \tag{25}$$

Here $\hat{T}\left(1,\hat{z},\hat{t}\right)$ is the temperature at the outer surface of the plug. The dimensionless heat transfer coefficient at the inner surface is

$$Nu_{p,o} = \frac{h_{p,o} r_o}{k} \tag{26}$$

where $h_{p,o}$ is the dimensional heat transfer coefficient. In the present work, the outer radius r_o is used as the length scale in Nusselt numbers, as r_o is the length scale in all other dimensionless parameters. Hence, the trends of Nusselt numbers changing with the plug dimensionless parameters reflect the trends of the dimensional heat transfer coefficients changing with the dimensional parameters of the plug. This will facilitate the discussion and explanation in the present work.

How does $Nu_{p,o}$ change with time when the heat transfer is fully developed? If we replace $\widehat{T}_a$ in Eq. (20) with the temperature on the outer surface $\widehat{T}\left(1,\hat{z},\hat{t}\right)$, and then substitute Eq. (20) into Eq. (25) for $\widehat{T}$, we see that the local Nusselt number $Nu_{p,o}=(\partial f/\partial\hat{r})_{\hat{r}=1}$, which is independent of $\hat{t}$.

Applying Eq. (23) to Eq. (25) gives

$$-1=Nu_{p,o}\left[\hat{T}(1,\hat{z},\hat{t})-\hat{T}_{p,m}(\hat{t})\right] \tag{27}$$

As discussed above, $Nu_{p,o}$ is independent of time. We take the time derivative of Eq. (27), and get

$$\frac{\partial\hat{T}(1,\hat{z},\hat{t})}{\partial t}=\frac{d\hat{T}_{p,m}}{dt} \tag{28}$$

Now we replace $\widehat{T}_a$ with $\widehat{T}\left(1,\hat{z},\hat{t}\right)$ in Eq. (21), and then combine Eqs. (21) and (28), we get

$$\frac{\partial\hat{T}}{\partial t}=\frac{d\hat{T}_{p,m}}{dt} \tag{29}$$

Substituting Eq. (23) into Eq. (19) gives

$$\frac{d\hat{T}_{p,m}}{d\hat{t}}=\frac{2}{(1-\eta^2)Pe} \tag{30}$$

From Eqs. (29) and (30), the transient term in Eq. (15) can be replaced with a non-transient term. As a result, Eq. (15) becomes

$$\frac{2}{(1-\eta^2)Pe}+\frac{\hat{u}_r}{\hat{r}}\frac{\partial\left(\hat{T}\hat{r}\right)}{\partial\hat{r}}+\hat{u}_z\frac{\partial\hat{T}}{\partial\hat{z}}=\frac{1}{Pe}\left[\frac{1}{\hat{r}}\frac{\partial}{\partial\hat{r}}\left(\hat{r}\frac{\partial\hat{T}}{\partial\hat{r}}\right)+\frac{\partial^2\hat{T}}{\partial\hat{z}^2}\right] \tag{31}$$

which is the governing equation for the outer-flux condition. With the boundary conditions defined by Eqs. (16) and (23) and the velocity solutions given by Eqs. (5)–(7), Eq. (31) is numerically computed.

To evaluate the global heat transfer of the plug, we choose to use the average heat transfer coefficient, which is the average heat flux divided by the average temperature difference. Based on the local convection given by Eq. (27), the Nusselt number for the iso-flux condition at the outer surface is

$$\overline{Nu}_{p,o}=\frac{\bar{h}_{p,o}r_o}{k}=\left[\frac{1}{\hat{l}}\int_0^{\hat{l}}\hat{T}(1,\hat{z},\hat{t})d\hat{z}-\hat{T}_{p,m}\right]^{-1} \tag{32}$$

Here $\bar{h}_{p,o}$ is the average heat transfer coefficient at the outer surface.

The dependency of the numerical computation on the mesh resolution is tested using a plug ($\eta=0.05,\ \hat{l}=2,\ Pe=200$) under the outer-flux condition. Table 1 lists the tested resolutions, which are shown in the form of the number of elements in $\hat{r}$ followed by the number of elements in $\hat{z}$. The number of elements in $\hat{z}$ is maintained twice that in $\hat{r}$, because $\hat{l}>1-\eta$ for most of the plugs studied in the present work. As the meshing resolution increases, the change of the Nusselt number $\overline{Nu}_{p,o}$ decreases. Further increasing from 200×400 to 300×600, the change of $\overline{Nu}_{p,o}$ is only 1.4%. Hence, the resolution 200×400 is used throughout the present work.

Since there are no heat transfer results of concentric plugs, either numerical or experimental, available in literature, the present method, i.e. Eqs. (5)–(7), (16), (23), and (31), is validated against the reported results of a liquid plug in a circular pipe ($\hat{l}=4,\ Pe=4,16,64,100$) with iso-flux wall condition [24]. We apply the present method to a concentric plug with the same values of $\hat{l}$ and Pe as the circular plug but a very small inner radius $\eta=0.01$, such that the concentric plug approximates to the circular plug. The previous study [24] focuses on the transient process, and the values of Nusselt number at $\hat{t}=40$, which can be considered fully developed, are used for validation. Different from the present work, the Nusselt number in the previous study is based on the diameter of the pipe. Hence, the results of $2\overline{Nu}_{p,o}$ from the present work are compared to the data reported in the previous study. Table 2 shows that the difference is between 1% and 5%.

For the continuous flow in a circular tube annulus with the outer-flux condition, the Nusselt number, Nu_o, can be calculated using Eq. (A9) and (A13).

Fig. 3 shows the Nusselt number of the plug under the outer-flux condition $\overline{Nu}_{p,o}$ versus the inner radius η. Comparison is made with the continuous flow under the same thermal wall condition.

Table 2
Validation of the present method against a previous study [24]. The plug length $\hat{l}=4$.

Pe	4	16	64	100
$2\overline{Nu}_{p,o}$ for $\eta=0.01$	8.02	16.51	25.38	27.50
Nusselt number in [24]	7.60	15.93	25.70	27.04

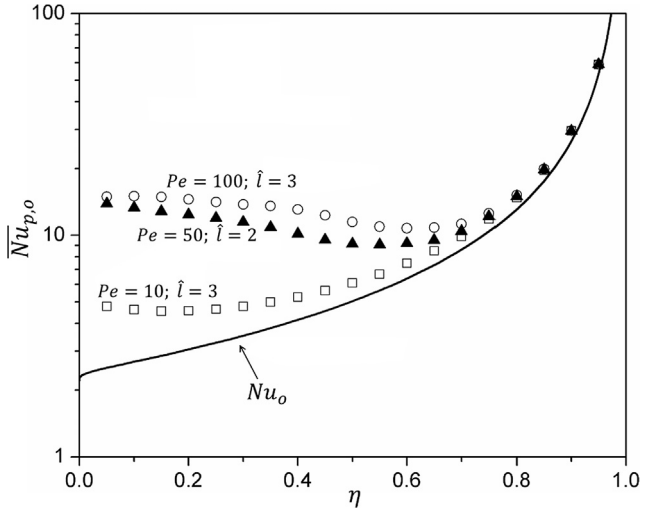

Fig. 3. The Nusselt number for plugs with the outer-flux condition, $\overline{Nu}_{p,o}$ given by Eq. (32) versus the inner radius η. Comparison is made to the Nusselt number for continuous flow Nu_o given by Eqs. (A9) and (A13).

Table 1
Test of mesh dependency for a plug ($\eta=0.05,\ \hat{l}=2,\ Pe=200$) under the outer-flux condition.

Meshresolution	25* × 50**	75 × 150	100 × 200	200 × 400	300 × 600
$\overline{Nu}_{p,o}$	15.77	17.23	17.67	18.28	18.53

* The number of elements in $\hat{r}$.
** The number of elements in $\hat{z}$.

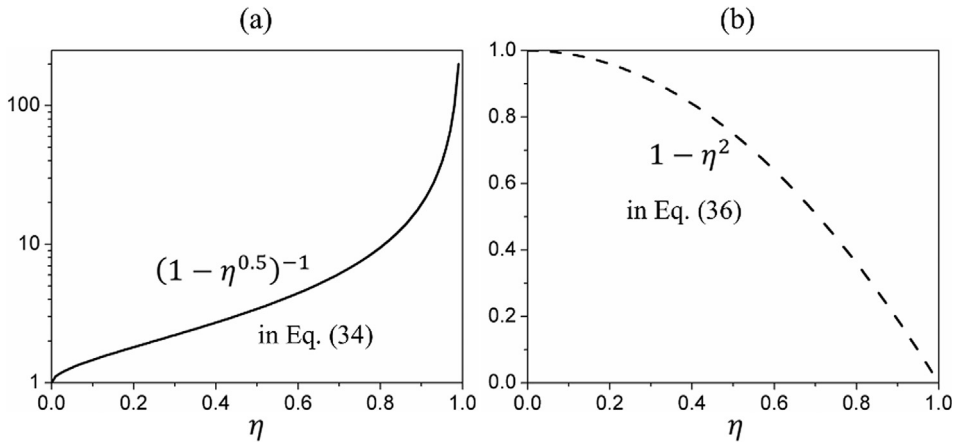

Fig. 4. The heat transport mechanisms in a plug with the outer-flux condition. (a) The trend of the boundary layer transport changing with the inner radius; (b) The trend of the radial transport changing with the inner radius.

The plug shows heat transfer enhancement over the continuous flow. The enhancement varies with the plug properties: η, Pe, and $\widehat{l}$. For $\eta \to 1$, the aspect ratio of the plug $\widehat{l}/(1-\eta) \to \infty$, which means the plug is changing toward the continuous flow. Hence, as $\eta \to 1$, the plug behaves like the continuous flow.

Below we will try to explain the trends shown in Fig. 3. The heat transfer between the pipe wall and the plug can be considered to have the involvement of two mechanisms. One mechanism is the heat transfer through the boundary layer, referred to as the *boundary-layer transport*. This is the primary mechanism of convection heat transfer for continuous flow. The other one is the flow in radial direction due to the vortex circulation, which is referred to as *radial transport*. Both factors contribute to the heat transfer, which, to facilitate further discussion below, can be written as $\overline{Nu}_{p,o}\ \left(\overline{Nu}_{p,o,b}+\overline{Nu}_{p,o,c}\right)$. Here $\overline{Nu}_{p,o,b}$ and $\overline{Nu}_{p,o,c}$ represent the contributions from the boundary-layer transport and the radial transport, respectively.

According to the Reynolds analogy, the thermal boundary layer can be discussed based on the velocity boundary layer. As shown in Fig. 1b, the outer vortex is located between r_o and r_c. The average velocity gradient at the outer wall can be expressed as

$$-\frac{1}{l}\int_0^l \left.\frac{\partial u_z}{\partial r}\right|_{r=r_o} dz \sim \frac{U}{(r_o-r_c)/2} \tag{33}$$

Multiplying Eq. (33) through by r_o/U and considering the Reynolds analogy, we write the relation between the Nusselt number and the dimensionless velocity gradient as

$$\overline{Nu}_{p,o,b} \propto -\frac{1}{\hat{l}}\int_0^{\hat{l}} \left.\frac{\partial \hat{u}_z}{\partial \hat{r}}\right|_{\hat{r}=1} d\hat{z} \sim \frac{2}{1-\eta^{0.5}} \tag{34}$$

where Eq. (3) has been used.

The involvement of the radial transport can be evaluated using

$$\overline{Nu}_{p,o,c}\frac{k}{r_o}r_o \propto Q'\rho c_p \tag{35}$$

Putting Eq. (4) into Eq. (35) gives

$$\overline{Nu}_{p,o,c} \propto 0.1973(1-\eta^2)\hat{l}^{-1}Pe \tag{36}$$

To show the effects of η in the two heat transfer mechanisms discussed above, the term $\left(1-\eta^{0.5}\right)^{-1}$ in Eq. (34) is plotted versus η in Fig. 4a, while the term $1-\eta^2$ in Eq. (36) is plotted in Fig. 4b. Fig. 4a shows that the boundary layer transport at the outer surface increases with increasing η. The trend looks similar to the trends of the plug and continuous flow in Fig. 3, particularly to the trend of the Nusselt number of the continuous flow. Fig. 4b shows the radian transport increases with decreasing η. Based on Figs. 3 and 4, the heat transfer of the continuous flow follows the trend of the boundary layer transport. The deviation of the plug from the continuous flow in Fig. 3, which is the heat transfer enhancement, can be attributed to the radial transport as shown in Fig. 4b. From Eq. (36), the enhancement must be a function of η, Pe, and $\widehat{l}$.

Here we discuss the effects of the plug length and the Peclet number on the heat transfer of the plug. From Eqs. (34) and (36), the plug length appears in the radial transport but not in the boundary layer transport. Since the plug length appears as $1/\widehat{l}$ in Eq. (36), Fig. 5 plots the Nusselt number versus $1/\widehat{l}$. Although the trend is not linear, it is clear that the heat transfer increases with the $1/\widehat{l}$. Reducing the plug length increases the circulation rate per unit plug length, thereby increasing the radial transport. As a result, the heat transfer enhancement is improved. One can also see that the effect of the plug length diminishes for large η and small Pe, For which the vortex circulation is weak.

From Eqs. (34) and (36), Pe appears only in the radial transport. The effect of the Peclet number can be observed from Fig. 6, which

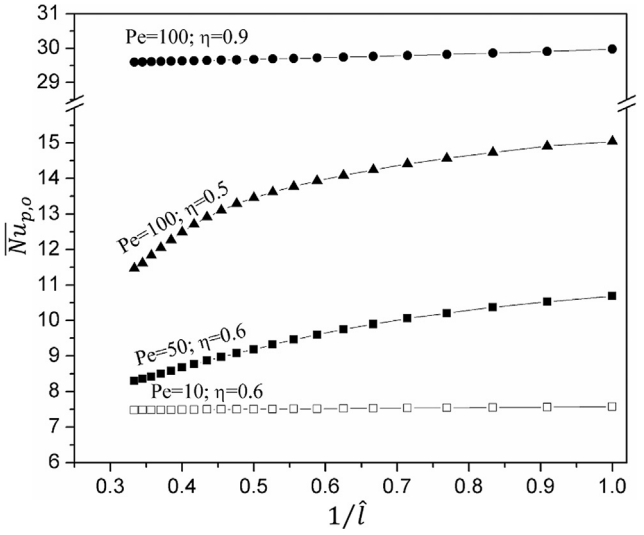

Fig. 5. The Nusselt number for plugs with the outer-flux condition, $\overline{Nu}_{p,o}$ given by Eq. (32) versus $1/\widehat{l}$.

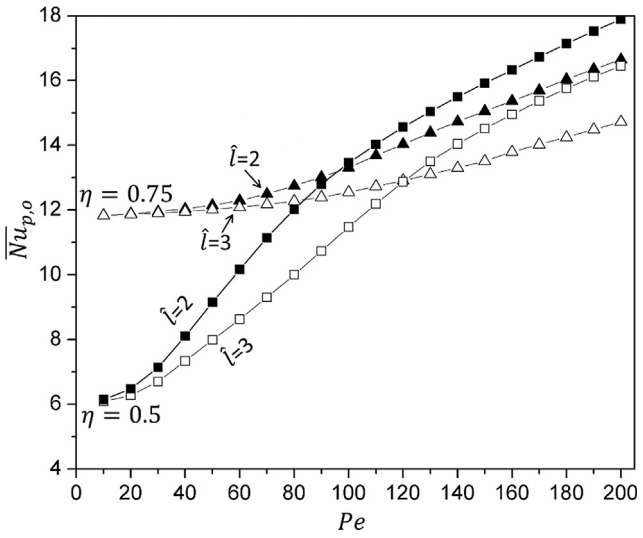

Fig. 6. The Nusselt number for plugs with the outer-flux condition, $\overline{Nu}_{p,o}$ given by Eq. (32) versus the Peclet number of the plug *Pe*.

shows the Nusselt number versus *Pe*. Overall, the Nusselt number increases with increasing *Pe*. When *Pe* is small, the plugs with $\eta = 0.75$ show better heat transfer than those with $\eta = 0.5$. This is because, for small *Pe*, the boundary layer transport is dominant, while the radial transport is insignificant. As *Pe* increases, the radial transport becomes significant, and the plugs with $\eta = 0.5$ show superior heat transfer because of their higher radial transport than those with $\eta = 0.75$. The discussion here can be combined with Figs. (3) and (5) for better understanding.

3.2. Inner-flux condition

The uniform heat flux is maintained at the inner surface, while the outer surface is insulated. The heat transfer at the wall-fluid interface is

$$-\left.\frac{\partial \hat{T}}{\partial \hat{r}}\right|_{\hat{r}=\eta} = Nu_{p,i}\left[\hat{T}(\eta,\hat{z},\hat{t}) - \hat{T}_{p,m}(\hat{t})\right] \tag{37}$$

Here $\hat{T}\left(\eta,\hat{z},\hat{t}\right)$ is the temperature at the inner surface of the plug. The dimensionless heat transfer coefficient at the inner surface is

$$Nu_{p,i} = \frac{h_{p,i} r_o}{k} \tag{38}$$

where $h_{p,i}$ is the dimensional heat transfer coefficient. Similar to the discussion in Section 3.1, it can be proved that for fully developed heat transfer, the Nusselt number $Nu_{p,i}$ is independent of time.

Applying Eq. (24) to Eq. (37) gives

$$1 = Nu_{p,i}\left[\hat{T}(\eta,\hat{z},\hat{t}) - \hat{T}_{p,m}(\hat{t})\right] \tag{39}$$

Taking steps similar to Eqs. (28)–(30), for fully developed heat transfer under the outer-flux condition, we obtain

$$\frac{\partial \hat{T}}{\partial \hat{t}} = \frac{d\hat{T}_{p,m}}{dt} = \frac{2\eta}{(1-\eta^2)Pe} \tag{40}$$

Replacing the transient term in Eq. (15) with Eq. (40), we rewrite the governing equation as

$$\frac{2\eta}{(1-\eta^2)Pe} + \frac{\hat{u}_r}{\hat{r}}\frac{\partial\left(\hat{T}\hat{r}\right)}{\partial \hat{r}} + \hat{u}_z\frac{\partial \hat{T}}{\partial \hat{z}} = \frac{1}{Pe}\left[\frac{1}{\hat{r}}\frac{\partial}{\partial \hat{r}}\left(\hat{r}\frac{\partial \hat{T}}{\partial \hat{r}}\right) + \frac{\partial^2 \hat{T}}{\partial \hat{z}^2}\right] \tag{41}$$

which is the governing equation for the inner-flux condition. With the boundary conditions defined by Eqs. (16) and (24) and the velocity solutions given by Eqs. (5)–(7), Eq. (41) is numerically computed.

To evaluate the global heat transfer of the entire plug, the average Nusselt number is used, which is given by

$$\overline{Nu}_{p,i} = \frac{\bar{h}_{p,i} r_o}{k} = \left[\frac{1}{\hat{l}}\int_0^{\hat{l}} \hat{T}(\eta,\hat{z},\hat{t})d\hat{z} - \hat{T}_{p,m}\right]^{-1} \tag{42}$$

Here $\bar{h}_{p,i}$ is the average heat transfer coefficient.

For the continuous flow in a circular tube annulus with inner-flux condition, the Nusselt number, Nu_i, can be calculated using Eqs. (A14) and (A18).

Fig. 7 shows the Nusselt number of the plug, $\overline{Nu}_{p,i}$, versus the inner radius, η, for the inner-flux condition. The heat transfer of the plug is compared with the heat transfer of the continuous flow. Generally, the plug shows heat transfer enhancement over the continuous flow. However, the enhancement diminishes as the annular pipe changes toward a circular pipe, i.e. $\eta \to 0$. Similar trend is visible when the annular pipe changes toward two parallel plates, i.e. $\eta \to 1$. As $\eta \to 1$, the plug approaches the continuous flow. For both the plug flow and the continuous flow, the relation of the heat transfer versus the inner radius does not show a monotonic trend. The Nusselt numbers increases for both $\eta \to 0$ and for $\eta \to 1$.

To explain the trends in Fig. 7, here we consider the boundary layer transport and the radial transport for the inner-flux condition. Similar to the discussion in Section 3.1, we write $\overline{Nu}_{p,i}$ $(\overline{Nu}_{p,i,b} + \overline{Nu}_{p,i,c})$. Here $\overline{Nu}_{p,i,b}$ and $\overline{Nu}_{p,i,c}$ represent the contributions from the boundary-layer transport and the radial transport, respectively. Considering the inner vortex in the plug as shown in Fig. 1b, we can write the velocity gradient at the inner surface as

$$\frac{1}{l}\int_0^{l}\left.\frac{\partial u_z}{\partial r}\right|_{r=r_i} dz \sim \frac{U}{(r_c - r_i)/2} \tag{43}$$

From Eqs. (3) and (43), the contribution of the boundary layer transport can be shown by

$$\overline{Nu}_{p,i,b} \propto \frac{1}{\hat{l}}\int_0^{\hat{l}}\left.\frac{\partial \hat{u}_z}{\partial \hat{r}}\right|_{\hat{r}=\eta} d\hat{z} \sim \frac{2}{\eta^{0.5} - \eta} \tag{44}$$

For the inner-flux condition, the radial transport is

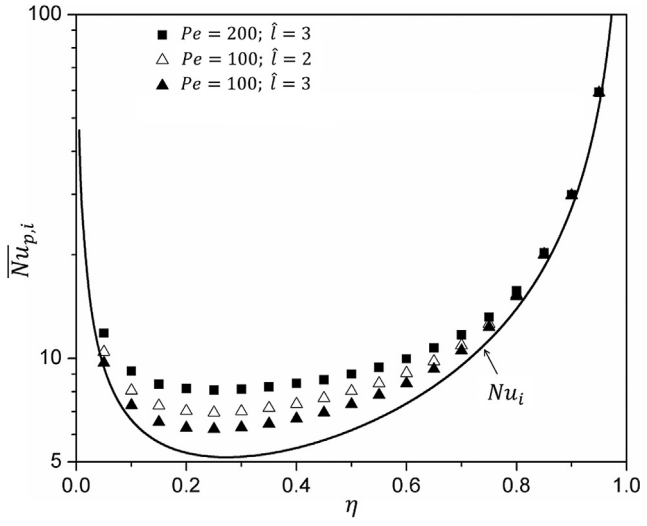

Fig. 7. The Nusselt number for plugs with the inner-flux condition, $\overline{Nu}_{p,i}$ given by Eq. (42) versus the inner radius η. Comparison is made to the Nusselt number for continuous flow Nu_i given by Eqs. (A14) and (A18).

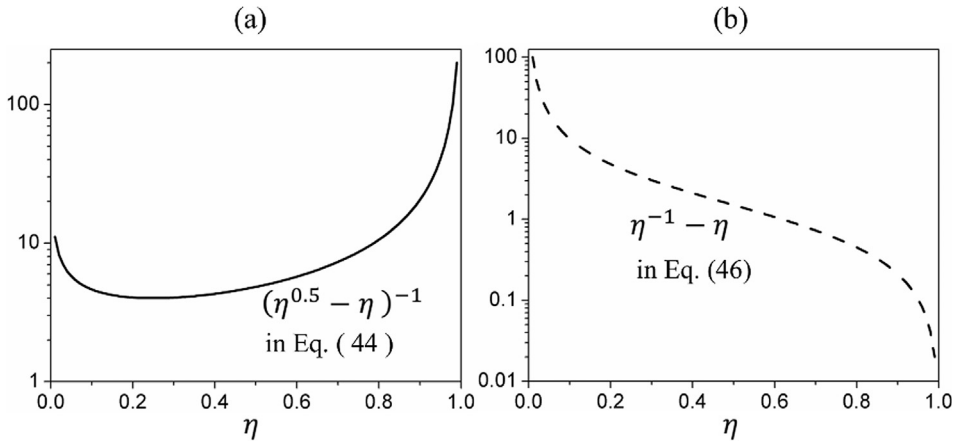

Fig. 8. The heat transport mechanisms in a plug with the inner-flux condition. (a) The trend of the boundary layer transport changing with the inner radius; (b) The trend of the radial transport changing with the inner radius.

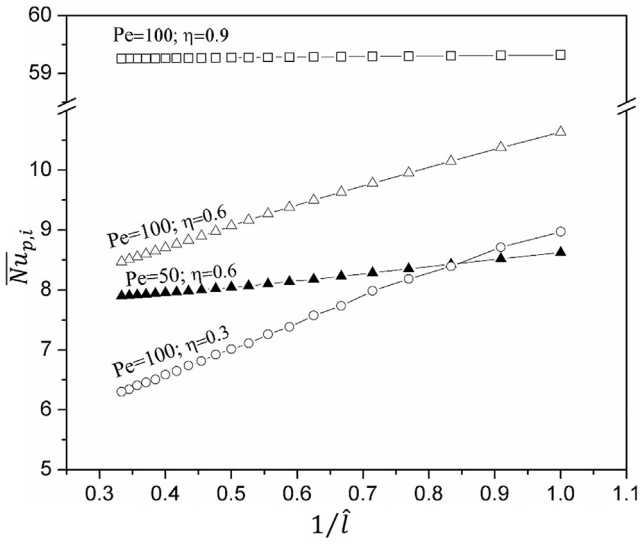

Fig. 9. The Nusselt number for plugs with the inner-flux condition, $\overline{Nu}_{p,i}$ given by Eq. (42) versus $1/\hat{l}$.

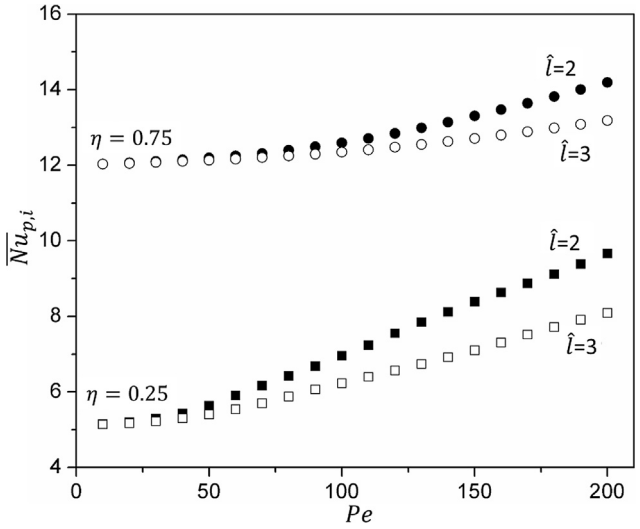

Fig. 10. The Nusselt number for plugs with the inner-flux condition, $\overline{Nu}_{p,i}$ given by Eq. (42) versus the Peclet number of the plug *Pe*.

$$\overline{Nu}_{p,i,c}\frac{k}{r_o}r_i \propto Q'\rho c_p \tag{45}$$

Putting Eq. (4) into Eq. (45)) gives

$$\overline{Nu}_{p,i,c} \propto 0.1973\left(\frac{1}{\eta}-\eta\right)\hat{l}^{-1}Pe \tag{46}$$

The effect of η on the boundary layer transport is shown in Fig. 8a by plotting the term $(\eta^{0.5}-\eta)^{-1}$ versus η. The trend shown in Fig. 8a is similar to that observed in Fig. 7. For the radian transport, $1-\eta^2$ is plotted versus η in Fig. 8b. The radial transport decreases toward zero as $\eta \to 1$, and increases with decreasing η. Based on Figs. 7 and 8, the heat transfer is primarily driven by the boundary layer transport, while the radial transport is the major cause for the heat transfer enhancement over the continuous flow. However, for $\eta \to 0$ (i.e. the heat source area is shrinking to disappear), it is difficult to relate the steep increase of the radial transport shown in Fig. 8b to the diminishing enhancement shown in Fig. 7.

From Fig. 7 we already observe that the length of the plug affects the heat transfer enhancement of the plug. According to Eq. (46), the Nusselt number is plotted versus $1/\hat{l}$ in Fig. 9. The heat transfer increases with increasing $1/\hat{l}$. The shorter the plug, the more circulation per unit length in the plug, which results in more radial transport. The slopes of the data curves in Fig. 9 vary with *Pe* and η, which can be explained by Eq. (46). The higher the Peclet number *Pe*, the more significantl effect of $\hat{l}$. For large radius ratio, for example $\eta = 0.9$, the effect of the plug length becomes insignificant.

Figs. 7 and 9 have shown that the heat transfer is also dependent on the Peclet number. Fig. 10 shows the Nusselt number of the plug versus the Peclet number. The heat transfer increases with increasing *Pe*, due to the increase of the radial transport. The slopes for $\eta = 0.25$ are higher than those for $\eta = 0.75$, and the slopes for $\hat{l} = 2$ are higher than those for $\hat{l} = 3$. Both can be explained by Eq. (46).

4. Isothermal wall condition

Fig. 2c shows a plug moving in an annular pipe with two different constant temperatures at the inner and outer surfaces of the

plug, and the wall condition is given in Eq. (11). To specifically define the dimensionless temperature given by Eq. (14), we choose the inner surface temperature as the reference temperature, i.e. $T_{ref} = T_i$, and the difference between the two wall temperatures as the characteristic temperature difference, i.e. $\Delta T_{std} = T_o - T_i$. As a result, we have

$$\hat{T} \equiv \frac{T - T_i}{T_o - T_i} \tag{47}$$

Accordingly, the dimensionless form of Eq. (11) is

$$\hat{T}(\eta, \hat{z}, \hat{t}) = 0; \quad \hat{T}(1, \hat{z}, \hat{t}) = 1 \tag{48}$$

Now we apply the two constant temperatures to Eq. (21) by letting $\widehat{T}_a = \widehat{T}\left(\eta, \widehat{z}, \widehat{t}\right)$ and $\widehat{T} = \widehat{T}\left(1, \widehat{z}, \widehat{t}\right)$, and we get

$$\frac{d\hat{T}_{p,m}}{d\hat{t}} = 0 \tag{49}$$

Then we apply Eq. (49) and $\widehat{T}_a = \widehat{T}\left(\eta, \widehat{z}, \widehat{t}\right)$ to Eq. (21), and get

$$\frac{\partial \hat{T}}{\partial \hat{t}} = 0 \tag{50}$$

Eq. (50) indicates that the fully developed heat transfer for a concentric plug with two constant boundary temperatures must be steady state heat transfer. The governing equation given by Eq. (15) reduces to

$$\frac{\hat{u}_r}{\hat{r}} \frac{\partial\left(\hat{T}\hat{r}\right)}{\partial \hat{r}} + \hat{u}_z \frac{\partial \hat{T}}{\partial \hat{z}} = \frac{1}{Pe}\left[\frac{1}{\hat{r}} \frac{\partial}{\partial \hat{r}}\left(\hat{r} \frac{\partial \hat{T}}{\partial \hat{r}}\right) + \frac{\partial^2 \hat{T}}{\partial \hat{z}^2}\right] \tag{51}$$

Hence, the fully developed heat transfer of a liquid plug in an annular pipe with isothermal wall condition can be obtained by numerically computing Eq. (51) with the velocity solutions given by Eqs. (5)–(7) and the boundary conditions defined by Eqs. (16) and (48).

The heat transfer can be assessed by introducing an overall heat transfer coefficient h_p based on the heat transfer area at the outer surface, which can be written as

$$-r_o k \left.\frac{\partial T}{\partial r}\right|_{r=r_o} = h_p r_o (T_i - T_o) \tag{52}$$

From Eqs. (47) and (52), the dimensionless overall heat transfer coefficient is

$$Nu_p = \frac{h_p r_o}{k} = \left.\frac{\partial \hat{T}}{\partial \hat{r}}\right|_{\hat{r}=1} \tag{53}$$

Fig. 11 shows the Nusselt number versus the inner radius in comparison with the continuous flow. As discussed in the Appendix A, the fully developed heat transfer of continuous flow under the isothermal condition is heat conduction only, and the Nusselt number is given by Eq. (A25). As compared to the continuous flow, the plug shows heat transfer enhancement due to the radial transport. Fig. 11 shows that the enhancement diminishes for $\eta \to 1$, as the plug with large aspect ratio behaves like the continuous flow.

To better show the effects of the other two parameters $\widehat{l}$ and Pe on the heat transfer enhancement, the ratio of Nusselt number of the plug to the continuous flow, Nu_p/Nu, is presented. Fig. 12 shows the effect of the plug length by plotting the enhancement

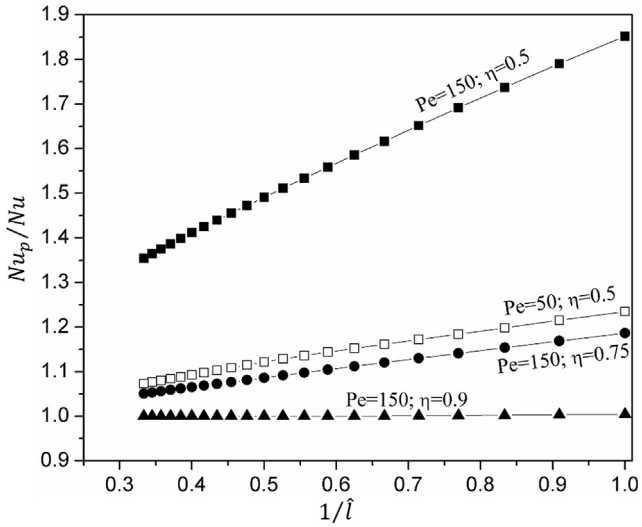

Fig. 12. The ratio of Nusselt number of the plug to the continuous flow, Nu_p/Nu, for the isothermal condition versus $1/\widehat{l}$. Nu_p and Nu are given by Eq. (53) and Eq. (A25), respectively.

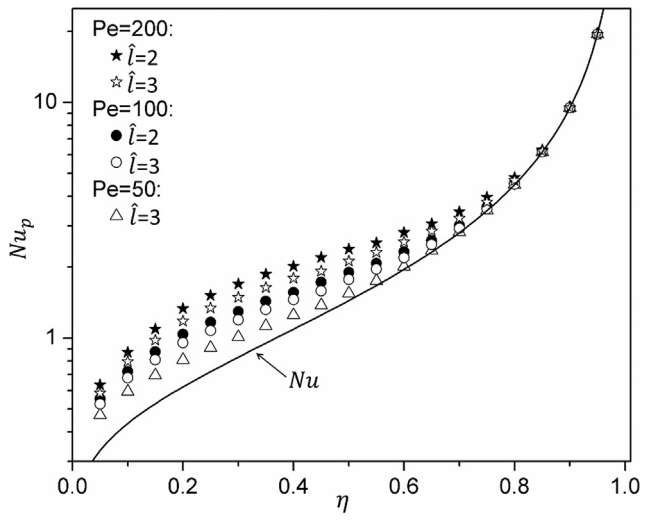

Fig. 11. The Nusselt number for plugs with the isothermal condition Nu_p given by Eq. (53) versus the inner radius η. Comparison is made to the Nusselt number for continuous flow Nu given by Eq. (A25).

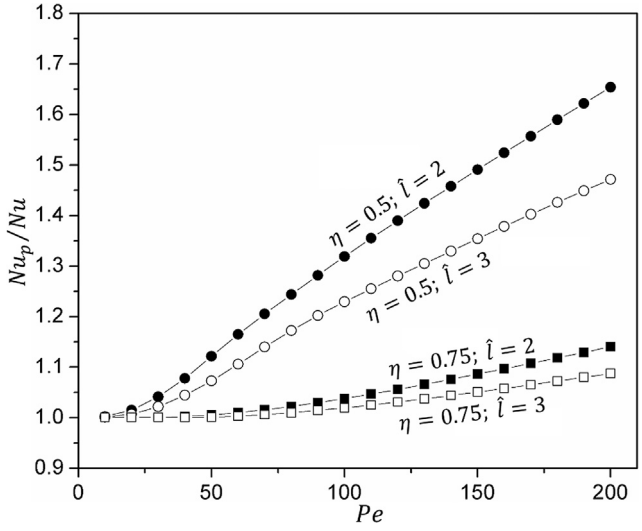

Fig. 13. The ratio of Nusselt number of the plug to the continuous flow, Nu_p/Nu, for the isothermal condition versus the Peclet number Pe. Nu_p and Nu are given by Eqs. (53) and (A25), respectively.

versus $1/\hat{l}$. Clearly, the shorter the plug, the more enhancement of heat transfer. The enhancement shows linear relationship with $1/\hat{l}$, and the slope varies with η and *Pe*. The effect of *Pe* on the enhancement is shown in Fig. 13. Increasing the Peclet number causes the radial transport to increase, which results in more enhancement. For small values of *Pe*, the ratio of Nusselt number approaches unity, because of the decrease of the radian transport.

5. Conclusions

The fully developed heat transfer of a liquid plug moving in a tube annulus is studied for three types of thermal wall conditions. The heat transfer governing equation is numerically solved based on the velocity solutions developed in the previous study. It has been shown that the transient term in the governing equation can be replaced with a non-transient term so that the fully developed heat transfer can be numerically computed using the non-transient equation. It has been shown that the heat transfer performance of the plug flow can be explained based on two heat transfer mechanisms, boundary layer transport and radial transport. The heat transfer of the liquid plug is found to be superior to the continuous flow if the plug has small inner radius, short length, and/or large Peclet number. The heat transfer enhancement of the plug over the continuous flow is attributed to the radial transport of the plug, and the radial transport increases with decreasing the inner radius, decreasing the plug length, and increasing the Peclet number.

Declaration of Competing Interest

The authors declared that there is no conflict of interest.

Acknowledgements

The authors thank the Natural Sciences and Engineering Research Council of Canada (NSERC) for support.

Appendix A. Continuous flow in a circular tube annulus

In this Appendix, the fully developed heat transfer of the continuous flow in an annular pipe will be analytically solved for three types of thermal wall conditions, and Nusselt numbers will be derived. A fully developed continuous flow in a tube annulus is shown in Fig. A1. Different from the plug flow analysis, here we consider the Euler frame of reference, in which the mean velocity of the flow is U. We still use the dimensionless temperature defined by Eq. (14). Both the flow and thermal conditions are steady, which means $\partial\hat{T}/\partial\hat{t}=0$, $\partial\hat{u}_r/\partial\hat{t}=0$, and $\partial\hat{u}_z/\partial\hat{t}=0$. The fully developed hydrodynamics means $\partial\hat{u}_r/\partial\hat{z}=0$ and $\partial\hat{u}_z/\partial\hat{z}=0$. As a result, $\hat{u}_r=0$, and $\hat{u}_z$ is a function of $\hat{r}$ only.

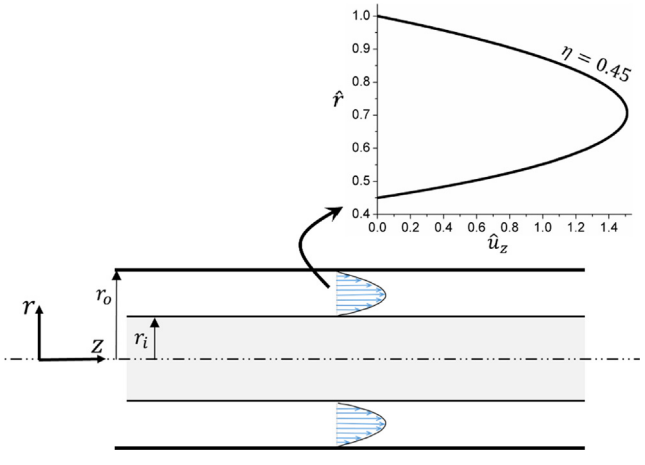

Fig. A1. Fully developed continuous flow in a tube annulus.

Hence, Eq. (15) reduces to

$$\hat{u}_z\frac{\partial\hat{T}}{\partial\hat{z}}=\frac{1}{Pe}\frac{1}{\hat{r}}\frac{\partial}{\partial\hat{r}}\left(\hat{r}\frac{\partial\hat{T}}{\partial\hat{r}}\right) \tag{A1}$$

Here we have dropped the axial conduction $\partial^2\hat{T}/\partial\hat{z}^2$ due to its relative insignificance as compared to the radial conduction. The velocity profile is given by [34]

$$\hat{u}_z=A\hat{r}^2+B\ln\hat{r}-A \tag{A2}$$

where

$$A=\frac{2\ln\eta}{\eta^2(1-\ln\eta)-(1+\ln\eta)};\quad B=\frac{2(1-\eta^2)}{\eta^2(1-\ln\eta)-(1+\ln\eta)} \tag{A3}$$

As an example, Eq. (A2) is plotted in Fig. A1 for $\eta=0.45$. We will solve Eq. (A1) for the three thermal wall conditions defined by Eqs. (23), (24), and (48).

First, we need to define the fully developed heat transfer so that we will replace the advection term in Eq. (A1) with a term independent of $\hat{z}$. We integrate Eq. (A1) over the cross-section of the flow, and get

$$\frac{d}{d\hat{z}}\int_\eta^1\hat{u}_z\hat{T}2\pi\hat{r}d\hat{r}=\frac{1}{Pe}\left(2\pi\frac{\partial\hat{T}}{\partial\hat{r}}\bigg|_{\hat{r}=1}-2\pi\eta\frac{\partial\hat{T}}{\partial\hat{r}}\bigg|_{\hat{r}=\eta}\right) \tag{A4}$$

In view of the term on the left hand side, we defined advection mean temperature, which is

$$\hat{T}_m=\frac{1}{\pi(1-\eta^2)}\int_\eta^1\hat{u}\hat{T}2\pi\hat{r}d\hat{r} \tag{A5}$$

It follows from Eqs. (A4) and (A5) that

$$\frac{d\hat{T}_m}{d\hat{z}}=\frac{1}{1-\eta^2}\frac{2}{Pe}\left(\frac{\partial\hat{T}}{\partial\hat{r}}\bigg|_{\hat{r}=1}-\eta\frac{\partial\hat{T}}{\partial\hat{r}}\bigg|_{\hat{r}=\eta}\right) \tag{A6}$$

Similar to Eq. (20), the fully developed heat transfer of the continuous flow means the relative shape of the temperature profile at any location $\hat{z}$ is independent of $\hat{z}$. This statement can be expressed by

$$\frac{\hat{T}_a(\hat{r}_a,\hat{z})-\hat{T}(\hat{r},\hat{z})}{\hat{T}_a(\hat{r}_a,\hat{z})-\hat{T}_m(\hat{z})}=f(\hat{r},\hat{r}_a) \tag{A7}$$

where $\hat{T}_a$ is a local temperature at an arbitrary location $(\hat{r}_a,\hat{z})$. Taking the time derivative of Eq. (A7) gives

$$\frac{\partial\hat{T}}{\partial\hat{z}}=\frac{d\hat{T}_a}{d\hat{z}}+\frac{\hat{T}_a-\hat{T}}{\hat{T}_a-\hat{T}_m}\left(\frac{d\hat{T}_m}{d\hat{z}}-\frac{d\hat{T}_a}{d\hat{z}}\right) \tag{A8}$$

For the outer-flux condition, the Nusselt number is defined based on Eqs. (22) and (23), which is

$$Nu_o=\frac{h_o r_o}{k}=\left[\hat{T}_m(\hat{z})-\hat{T}(1,\hat{z})\right]^{-1} \tag{A9}$$

Taking steps similar to Eqs. (28) and (29) gives

$$\frac{\partial\hat{T}}{\partial\hat{z}}=\frac{d\hat{T}_m}{d\hat{z}}=\frac{1}{1-\eta^2}\frac{2}{Pe} \tag{A10}$$

Putting Eq. (A10) into Eq. (A1) gives the governing equation for the outer-flux condition, which is

$$\frac{2}{1-\eta^2}\left(A\hat{r}^2+B\ln\hat{r}-A\right)=\frac{1}{\hat{r}}\frac{\partial}{\partial\hat{r}}\left(\hat{r}\frac{\partial\hat{T}}{\partial\hat{r}}\right) \tag{A11}$$

Solving Eq. (A11) with Eq. (23) gives

$$\hat{T}(1,\hat{z})-\hat{T}=\frac{2}{1-\eta^2}\left(\frac{A}{16}\hat{r}^4+\frac{B}{4}\hat{r}^2\ln\hat{r}-\frac{A+B}{4}\hat{r}^2+\frac{A+B+2-2\eta^2}{4}\ln\hat{r}\right)\Big|_{\hat{r}}^{1} \tag{A12}$$

To obtain the Nusselt number defined in Eq. (A9), here we take the advection mean of Eq. (A12) by following the definition given by Eq. (A5). As a result, we get

$$\hat{T}_m-\hat{T}(1,\hat{z})=\frac{1}{\pi(1-\eta^2)}\int_\eta^1\hat{u}_z\left(\hat{T}-\hat{T}_o\right)2\pi\hat{r}d\hat{r}=\frac{2}{1-\eta^2}\left(\frac{3A}{16}+\frac{B}{4}\right)+$$

$$\frac{4}{(1-\eta^2)^2}\left\{\begin{array}{l}\left[\frac{25}{384}A^2+\frac{11}{72}AB+\frac{11}{128}B^2+\frac{1-\eta^2}{2}\left(\frac{3A}{16}+\frac{B}{4}\right)\right]-\\ \frac{A^2}{128}\eta^8-\frac{5A}{96}\eta^6\left(B\ln\eta-\frac{29}{30}B-A\right)-\\ \frac{\eta^4}{16}\left[B^2(\ln\eta)^2+\left(A^2-\frac{3}{2}B^2-AB\right)\ln\eta+\frac{3}{4}A^2+\frac{3}{8}B^2+\frac{5}{4}AB\right]-\\ \frac{(A+B)}{8}\eta^2\left[B(\ln\eta)^2-(A+B)\ln\eta+\frac{(A+B)}{2}\right]-\\ \frac{1-\eta^2}{2}\left[A\frac{\eta^4}{4}\left(\ln\eta-\frac{1}{4}\right)+B\frac{\eta^2}{2}(\ln\eta)^2-\frac{\eta^2}{2}(A+B)\left(\ln\eta-\frac{1}{2}\right)\right]\end{array}\right\} \tag{A13}$$

Hence, for continuous flow in an annular pipe with the outer-flux condition, the Nu_o can be calculated using Eqs. (A9) and (A13).

For the inner-flux condition, following Eqs. (22) and (24), respectively, we define the Nusselt number as

$$Nu_i=\frac{h_i r_o}{k}=\left[\hat{T}(\eta,\hat{z})-\hat{T}_m(\hat{z})\right]^{-1} \tag{A14}$$

Here h_i is the dimensional heat transfer coefficient. It should be noted that r_o is consistently used as the length scale.

Taking steps similar to Eqs. (28) and (29), we get

$$\frac{\partial\hat{T}}{\partial\hat{z}}=\frac{d\hat{T}_m}{d\hat{z}}=\frac{\eta}{1-\eta^2}\frac{2}{Pe} \tag{A15}$$

For the inner-flux condition, Eq. (A1) can be written as

$$\frac{2\eta}{1-\eta^2}\left(A\hat{r}^2+B\ln\hat{r}-A\right)=\frac{1}{\hat{r}}\frac{\partial}{\partial\hat{r}}\left(\hat{r}\frac{\partial\hat{T}}{\partial\hat{r}}\right) \tag{A16}$$

Solving Eq. (A16) with Eq. (24) gives

$$\hat{T}-\hat{T}(\eta,\hat{z})=\frac{2\eta}{1-\eta^2}\left(\frac{A}{16}\hat{r}^4+\frac{B}{4}\hat{r}^2\ln\hat{r}-\frac{A+B}{4}\hat{r}^2+\frac{A+B}{4}\ln\hat{r}\right)\Big|_{\eta}^{\hat{r}} \tag{A17}$$

To obtain the Nusselt number defined in Eq. (A14), here we take the advection-based mean of Eq. (A17) by following the definition given by Eq. (A5). As a result, we get

$$\hat{T}(\eta,\hat{z})-\hat{T}_m=\frac{1}{\pi(1-\eta^2)}\int_\eta^1\hat{u}_z\left[\hat{T}(\eta,\hat{z})-\hat{T}\right]2\pi\hat{r}d\hat{r}=$$

$$\frac{2\eta}{1-\eta^2}\left(\frac{A}{16}\eta^4+\frac{B}{4}\eta^2\ln\eta-\frac{A+B}{4}\eta^2+\frac{A+B}{4}\ln\eta\right)-$$

$$\frac{4\eta}{(1-\eta^2)^2}\left\{\begin{array}{l}\left(\frac{25}{384}A^2+\frac{11}{72}AB+\frac{11}{128}B^2\right)-\frac{A^2}{128}\eta^8-\frac{5A}{96}\eta^6\left(B\ln\eta-\frac{29}{30}B-A\right)-\\ \frac{\eta^4}{16}\left[B^2(\ln\eta)^2+\left(A^2-\frac{3}{2}B^2-AB\right)\ln\eta+\frac{3}{4}A^2+\frac{3}{8}B^2+\frac{5}{4}AB\right]-\\ \frac{(A+B)}{8}\eta^2\left[B(\ln\eta)^2-(A+B)\ln\eta+\frac{(A+B)}{2}\right]\end{array}\right\} \tag{A18}$$

Hence, for continuous flow in an annular pipe with the inner-flux condition, the Nusselt number Nu_i can be calculated using Eqs. (A14) and (A18)

The fully developed heat transfer of continuous flow in a circular tube annulus has been reported in data tables [33], where the Nusselt numbers are based on the hydraulic diameter, $2(r_o-r_i)$. The Nusselt numbers based on the outer radius can be converted to the Nusselt numbers based on the hydraulic dimeter using

$$Nu_{i,D_h}=2(1-\eta)Nu_i \tag{A19}$$

and

$$Nu_{o,D_h}=2(1-\eta)Nu_o \tag{A20}$$

In Fig. A2, the two Nusselt numbers, Nu_{i,D_h} and Nu_{o,D_h}, are plotted versus η using the solutions derived above. The derived solutions agree with the tabulated data [33]. With increasing η, the Nusselt number for the outer-flux condition, Nu_{o,D_h}, increases from 4.364, which is for continuous flow in a circular pipe, to 5.385, which is for continuous flow in two parallel plates. With increasing η, the Nusselt number for the outer-flux condition, Nu_{i,D_h}, decrease toward the Nusselt number for continuous flow in two parallel plates.

For continuous flow in a circular tube annulus with the isothermal wall condition given Eq. (48), the dimensionless temperature has been defined by Eq. (47). For fully developed heat transfer, from Eq. (A5), it can be shown that

$$\frac{\partial\hat{T}}{\partial\hat{z}}=\frac{d\hat{T}_m}{d\hat{z}}=0 \tag{A21}$$

As a result, Eq. (A1) reduces

$$\frac{1}{\hat{r}}\frac{\partial}{\partial\hat{r}}\left(\hat{r}\frac{\partial\hat{T}}{\partial\hat{r}}\right)=0 \tag{A22}$$

A fully thermally developed continuous flow under the isothermal condition only conducts heat. In other words, the convection here is conduction only, but no advection. The flow does not transport thermal energy in axial flow direction as shown in Eq. (A21), and there is no advection in radial direction as $\hat{u}_r=0$.

For the wall condition defined by Eq. (48), the solution to Eq. (A22) is

$$\hat{T}=\frac{\ln(\eta/\hat{r})}{\ln\eta} \tag{A23}$$

Similar to Eq. (52), we introduce an effective heat transfer coefficient based on the outer surface area, which can be written as

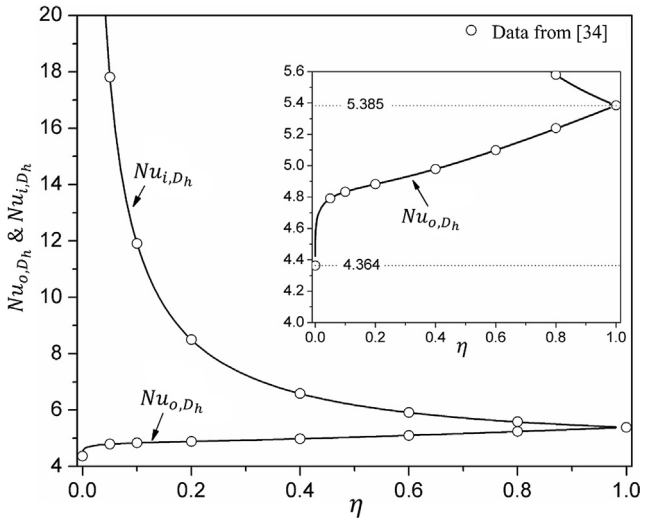

Fig. A2. Nusselt numbers based on the hydraulic diameter of the tube annulus for the inner-flux condition and the outer-flux condition. The inset figure provides a close-up of the outer-flux Nusselt number.

$$-r_o k\left.\frac{\partial T}{\partial r}\right|_{r=r_o} = hr_o(T_i - T_o) \tag{A24}$$

From Eq. (27), the Nusselt number for the fully developed heat transfer of continuous flow in a circular tube annulus with the isothermal condition is

$$Nu = \frac{hr_o}{k} = -\left.\frac{\partial \hat{T}}{\partial \hat{r}}\right|_{\hat{r}=1} = -\frac{1}{\ln\eta} \tag{A25}$$

Appendix B. Supplementary material

Supplementary data to this article can be found online at https://doi.org/10.1016/j.ijheatmasstransfer.2019.05.088.

References

[1] D.B. Tuckerman, R.F.W. Pease, High-performance heat sinking for VLSI, IEEE Electron Device Lett. 2 (1981) 126–129.
[2] S.S. Mehendale, A.M. Jacobi, R.K. Shah, Fluid flow and heat transfer at micro- and meso-scales with application to heat exchanger design, Appl. Mech. Rev. 53 (2000) 175–193.
[3] H.A. Mohammed, P. Gunnasegaran, N.H. Shuaib, Numerical simulation of heat transfer enhancement in wavy microchannel heat sink, Int. Commun. Heat Mass Transf. 38 (2011) 63–68.
[4] M. Dehghan, M. Daneshipour, M.S. Valipour, R. Rafee, S. Saedodin, Enhancing heat transfer in microchannel heat sinks using converging flow passages, Energy Convers. Manage. 92 (2015) 244–250.
[5] L. Chai, G.D. Xia, H.S. Wang, Numerical study of laminar flow and heat transfer in microchannel heat sink with offset ribs on sidewalls, Appl. Therm. Eng. 92 (2016) 32–41.
[6] W. Yuan, J. Zhao, C.P. Tso, T. Wu, W. Liu, T. Ming, Numerical simulation of the thermal hydraulic performance of a plate pin fin heat sink, Appl. Therm. Eng. 48 (2012) 81–88.
[7] J. Sivasamy, Z.Z. Che, T.N. Wong, N.T. Nguyen, L. Yobas, A simple method for evaluating and predicting chaotic advection in microfluidic slugs, Chem. Eng. Sci. 65 (2010) 5382–5391.
[8] Z.Z. Che, T.N. Wong, N.T. Nguyen, Heat transfer enhancement by recirculating flow within liquid plugs in microchannels, Int. J. Heat Mass Transf. 55 (2012) 1947–1956.
[9] Z.Z. Che, T.N. Wong, N.T. Nguyen, An analytical model for plug flow in microcapillaries with circular cross section, Int. J. Heat Fluid Flow 32 (2011) 1005–1013.
[10] T. Bandara, N.T. Nguyen, G. Rosengarten, Slug flow heat transfer without phase change in microchannels: a review, Chem. Eng. Sci. 126 (2015) 283–295.
[11] S.S. Leung, Y. Liu, D.F. Fletcher, B.S. Haynes, Heat transfer in well-characterised Taylor flow, Chem. Eng. Sci. 65 (2010) 6379–6388.
[12] S.S. Leung, R. Gupta, D.F. Fletcher, B.S. Haynes, Effect of flow characteristics on Taylor flow heat transfer, Ind. Eng. Chem. Res. 51 (2011) 2010–2020.
[13] Y.S. Lim, S.C. Yu, N.T. Nguyen, Flow visualization and heat transfer characteristics of gas–liquid two-phase flow in microtube under constant heat flux at wall, Int. J. Heat Mass Transf. 56 (2013) 350–359.
[14] P.A. Walsh, E.J. Walsh, Y.S. Muzychka, Heat transfer model for gas–liquid slug flows under constant flux, Int. J. Heat Mass Transf. 53 (2010) 3193–3201.
[15] J.A. Howard, P.A. Walsh, E.J. Walsh, Prandtl and capillary effects on heat transfer performance within laminar liquid–gas slug flows, Int. J. Heat Mass Transf. 54 (2011) 4752–4761.
[16] M.M.G. Eain, V. Egan, J. Punch, Local Nusselt number enhancements in liquid–liquid Taylor flows, Int. J. Heat Mass Transf. 80 (2015) 85–97.
[17] F. Houshmand, Y. Peles, Heat transfer enhancement with liquid–gas flow in microchannels and the effect of thermal boundary layer, Int. J. Heat Mass Transf. 70 (2014) 725–733.
[18] A.N. Asadolahi, R. Gupta, D.F. Fletcher, B.S. Haynes, CFD approaches for the simulation of hydrodynamics and heat transfer in Taylor flow, Chem. Eng. Sci. 66 (2011) 5575–5584.
[19] V. Talimi, Y.S. Muzychka, S. Kocabiyik, Numerical simulation of the pressure drop and heat transfer of two phase slug flows in microtubes using moving frame of reference technique, Int. J. Heat Mass Transf. 55 (2012) 6463–6472.
[20] K. Fukagata, N. Kasagi, P. Ua-arayaporn, T. Himeno, Numerical simulation of gas–liquid two-phase flow and convective heat transfer in a micro tube, Int. J. Heat Fluid Flow 28 (2007) 72–82.
[21] Z. Che, T.N. Wong, N.T. Nguyen, C. Yang, Three dimensional features of convective heat transfer in droplet-based microchannel heat sinks, Int. J. Heat Mass Transf. 86 (2015) 455–464.
[22] J. Zhang, D.F. Fletcher, W. Li, Heat transfer and pressure drop characteristics of gas–liquid Taylor flow in mini ducts of square and rectangular cross-sections, Int. J. Heat Mass Transf. 103 (2016) 45–56.
[23] R. Gupta, D.F. Fletcher, B.S. Haynes, CFD modelling of flow and heat transfer in the Taylor flow regime, Chem. Eng. Sci. 65 (2010) 2094–2107.
[24] Z. Che, T.N. Wong, N.T. Nguyen, Heat transfer in plug flow in cylindrical microcapillaries with constant surface heat flux, Int. J. Therm. Sci. 64 (2013) 204–212.
[25] Z. Che, T.N. Wong, N.T. Nguyen, C. Yang, Asymmetric heat transfer in liquid–liquid segmented flow in microchannels, Int. J. Heat Mass Transf. 77 (2014) 385–394.
[26] C. Hong, Y. Asako, K. Suzuki, Convection heat transfer in concentric micro annular tubes with constant wall temperature, Int. J. Heat Mass Transf. 54 (2011) 5242–5252.
[27] A.F. Khadrawi, A. Al-Shyyab, Slip flow and heat transfer in axially moving micro-concentric cylinders, Int. Commun. Heat Mass Transf. 37 (2010) 1149–1152.
[28] P. Naphon, Study on the exergy loss of the horizontal concentric micro-fin tube heat exchanger, Int. Commun. Heat Mass Transf. 38 (2011) 229–235.
[29] P. Naphon, T. Suchana, Heat transfer enhancement and pressure drop of the horizontal concentric tube with twisted wires brush inserts, Int. Commun. Heat Mass Transf. 38 (2011) 236–241.
[30] B.X. Wang, X.Z. Du, Condensation on the outside surface of a small/mini diameter tube for vapor flowing through a horizontal annulus surround by an adiabatic concentric tube, Int. J. Heat Mass Transf. 43 (2000) 1391–1398.
[31] M. Turkyilmazoglu, Anomalous heat transfer enhancement by slip due to nanofluids in circular concentric pipes, Int. J. Heat Mass Transf. 85 (2015) 609–614.
[32] Y. Cao, R. Li, A liquid plug moving in an annular pipe—flow analysis, Phys. Fluids 30 (2018) 093605.
[33] T.L. Bergman, A.S. Lavine, Fundamentals of Heat and Mass Transfer, Wiley, 2017.
[34] W.E. Langlois, M.O. Deville, Slow Viscous Flow, Springer, 1964.